Journal of Applied Mechanics and Technical Physics, Vol. 40, No. 5, 1999

NUMERICAL SIMULATION OF AEROSOL SAMPLING FROM AN AIR FLOW TO AN INPUT TUBE

A. A. Medvedev, N. N. Trusova, S. G. Chernyi,[1] and S. V. Sharov[1]

UDC 532.5

The processes of sampling (aspiration) to an input tube of an aspiration probe from an ambient air flow are studied numerically. The air flow is simulated on the basis of three-dimensional Navier–Stokes equations for an incompressible fluid. The method proposed allows calculation of the aspiration efficiency in the case of rather complicated shapes of the limiting trajectories of the particles. Dependences of the aspiration efficiency on the mean velocity of suction of air into the tube and the size of particles for a given free-stream velocity are obtained.

Introduction. Analysis of atmospheric and industrial aerosols involves aspiration of particles into samplers, whose output is connected to a metering device or a filter. A certain fraction of particles from the air sucked in does not enter the output metering device due to particle inertia (the particle trajectories do not coincide with the streamlines, particularly near the probe entrance, where the air velocity gradients are high) and deposition of particles in the inner duct of the probe [1]. Under certain conditions, "extraneous" particles from the air flowing around the probe can enter the probe due to their inertia. In addition, there exists an effect of secondary aspiration, when the particles deposited on or that recoil from the outer surface of the probe are sucked into the probe [1]. Thus, the concentration of particles in the metering device of the probe is usually different from the concentration in the air flow. The measure of distortion of the disperse composition of an aerosol during aspiration is the aspiration efficiency

$$A = c/c_0, \tag{1}$$

where c and c_0 are the mean-flow concentrations of a given fraction of the aerosol at the output of the probe (measured value) and in the volume of the air flow under study (true value), respectively. We distinguish the efficiency of external aspiration

$$A_e = c_e/c_0 \tag{2}$$

and internal aspiration

$$A_p = c/c_e. \tag{3}$$

Here c_e is the mean-flow concentration of particles of a given fraction at the probe input. Obviously, the total aspiration efficiency is

$$A = A_p A_e.$$

It is known that the value of A for the simplest and most frequently used probe with a cylindrical input tube can significantly differ from unity. Therefore, the design and use of these probes require quantitative data on aspiration efficiency.

Research Institute of Aerobiology, State Research Center of Virusology and Biotechnology "Vector," Novosibirsk Region, Kol'tsovo 633159. Institute of Computing Technologies, Siberian Division, Russian Academy of Sciences, Novosibirsk 630090. Translated from Prikladnaya Mekhanika i Tekhnicheskaya Fizika, Vol. 40, No. 5, pp. 113–122, September–October, 1999. Original article submitted December 10, 1997; revision submitted March 2, 1998.

0021-8944/99/4005-0877 $22.00 © 1999 Kluwer Academic/Plenum Publishers

Many papers deal with determining the errors of aspiration into a tube (see, for example, the review in [2]). However, for many cases, in particular, for aspiration into a tube oriented at an arbitrary angle to the flow, there are no reliable relationships between the aspiration efficiency and the governing parameters, such as the diameters of the particle d_p and the tube d, the velocity of air in the free stream W and in the tube V, and the angle between the flow direction and the tube axis α.

Semi-empirical relationships obtained in [2–5] on the basis of experimental data do not describe the entire range of the governing parameters; moreover, they agree poorly with each other. Experimental studies of the aspiration process have been mainly conducted using a method of comparison, where the aspiration efficiency was determined as the ratio of flow concentrations of a monodispersed aerosol measured by the probe examined and by the reference probe. In this case, the total aspiration efficiency is measured. It should be noted that this method is rather inaccurate because of the different variants of particle behavior when the particles are in contact with the outer and inner surfaces of the tube: the particles can stick, roll, blow off, recoil, or split. Thus, the measured concentration of the particles depends on the physicochemical properties of the particles and the tube surface. These factors are possibly responsible for the large scatter typical of data obtained by the method of comparison. The most reliable data on the efficiency of external aspiration were obtained by the method of limiting trajectories. The essence of this method is the use of optical methods to determine the particle trajectories closed on the butt-end edges of the probe and limiting the region of particles entering the probe. The diameter of the cross section limited by these trajectories far from the probe, i.e., the diameter of the tube of limiting trajectories, is the object of measurement in the method mentioned [6, 7].

If the flow is not parallel to the tube axis (particularly, at high values of the angle α), the cross section of the tube of limiting trajectories has a rather complicated shape, and it is very difficult to measure its area experimentally (the authors are not aware of any papers on this topic). Direct deposition of the particles on the inner surface of the tube can occur. Therefore, it is important not only to know the total aspiration efficiency, but also to take into account the effect of particle recoil and secondary aspiration.

Numerical studies allow one to take into account the effect of various factors. In particular, it is possible to calculate the aspiration efficiency for the following limiting cases: all particles that touched the solid wall do not enter the probe; the particles experience elastic reflection from the wall. It is possible to calculate the aspiration efficiency into a tube with an arbitrary orientation in an air flow only by solving three-dimensional equations that describe the air flow. A model incorporating viscous effects should be used for exact account of the special features arising in the flow, such as separations, vortices and their decompositions, and circulation.

Using the method of the solution of three-dimensional Navier–Stokes equations [8] effective for calculation of complex spatial flows, we simulated numerically a laminar air flow in the vicinity of the tube oriented at an angle of 90° to the external flow and inside the tube. The particle trajectories were calculated from the known velocity field by integration of the equations of particle motion. The tubes of the limiting trajectories were determined; these tubes enclosed particles that enter the input and output orifices of the tube. The efficiencies of external and total aspiration were found under the condition that all particles that touched the solid wall do not enter the probe. Dependences of the aspiration efficiency on the mean velocity of air suction into the tube and the particle size for a given free-stream velocity were obtained.

1. Numerical Method. We assume that the particle concentration in the air flow is low and the particles do not exert a noticeable effect on the velocity field, i.e., the reverse influence of the particles on the flow is ignored. We also assume that the air flow is laminar, steady, and incompressible. In this case, the aspiration process is simulated in two stages. At the first stage, we calculate the velocity field for the air near the tube and inside it by the numerical solution of three-dimensional incompressible Navier—Stokes equations. At the second stage, the trajectories of individual particles are calculated by integration of the equations of particle motion. We consider each of the stages in more detail.

1.1. *Calculation Method for the Velocity Field.* Three-dimensional equations of continuity and motion of an incompressible fluid, which are modified by introduction of a term with a derivative of pressure in time

[9, 10] into the continuity equation, are written in the form of integral conservation laws

$$\mathbf{R}\frac{\partial}{\partial t}\int\limits_V \mathbf{Q}\,dV = -\oint\limits_{\partial V}\mathbf{H}\cdot d\mathbf{S} + \int\limits_V \mathbf{F}\,dV, \tag{4}$$

where ∂V is a closed surface of an arbitrary fixed volume V, $d\mathbf{S} = \mathbf{n}\cdot dS$ is a surface element ∂V multiplied by the external unit normal $\mathbf{n}$ to it, $\mathbf{Q} = (p, u, v, w)^{\mathrm{t}}$, $\mathbf{R} = \mathrm{diag}\,(1/\varepsilon^2, 1, 1, 1)$, $\mathbf{F} = (0, f_x, f_y, f_z)^{\mathrm{t}}$, $\mathbf{H} = \mathbf{H}^{\mathrm{vis}} + \mathbf{H}^{\mathrm{in}}$, $\mathbf{H}^{\mathrm{vis}} = -1/\mathrm{Re}\,(0, \nabla u, \nabla v, \nabla w)^{\mathrm{t}}$, $\mathbf{H}^{\mathrm{in}} = (\mathbf{u}, u\mathbf{u}+p\mathbf{e}_1, v\mathbf{u}+p\mathbf{e}_2, w\mathbf{u}+p\mathbf{e}_3)^{\mathrm{t}}$, $\mathbf{u} = (u, v, w)$ is the velocity vector in Cartesian coordinates, p is the pressure, (f_x, f_y, f_z) is the vector of mass forces, $\mathbf{e}_1 = (1, 0, 0)$, $\mathbf{e}_2 = (0, 1, 0)$, and $\mathbf{e}_3 = (0, 0, 1)$ form the basis of a Cartesian coordinate system, ε^2 is the coefficient of artificial compressibility, and Re is the Reynolds number. System (4) is applied to calculate steady flows of an incompressible fluid by the pseudo-transient method.

The approximation of system (4) by the implicit method of finite volumes leads to the following difference equations:

$$\mathbf{R}\frac{\mathbf{Q}^{n+1}_{ijk} - \mathbf{Q}^{n}_{ijk}}{\Delta t}V_{ijk} = \mathbf{RHS}^{n+1}_{ijk},$$

$$\begin{aligned}\mathbf{RHS}^{n+1}_{ijk} = -[&(\mathbf{H}\cdot\mathbf{S})^{n+1}_{i+1/2} - (\mathbf{H}\cdot\mathbf{S})^{n+1}_{i-1/2} + (\mathbf{H}\cdot\mathbf{S})^{n+1}_{j+1/2} - (\mathbf{H}\cdot\mathbf{S})^{n+1}_{j-1/2} \\ &+(\mathbf{H}\cdot\mathbf{S})^{n+1}_{k+1/2} - (\mathbf{H}\cdot\mathbf{S})^{n+1}_{k-1/2}] + \mathbf{F}^{n}_{ijk}V_{ijk}.\end{aligned} \tag{5}$$

Here $\mathbf{Q}_{ijk}$ is the mean value of $\mathbf{Q}$ in the cell V_{ijk}, Δt is the time step, and $(\mathbf{H}\cdot\mathbf{S})^{n+1}_{i+1/2}$, $(\mathbf{H}\cdot\mathbf{S})^{n+1}_{j+1/2}$, and $(\mathbf{H}\cdot\mathbf{S})^{n+1}_{k+1/2}$ are the difference fluxes through the boundaries of the cell V_{ijk}. The vectors $\mathbf{S}_{i+1/2}$, $\mathbf{S}_{j+1/2}$ and $\mathbf{S}_{k+1/2}$ are the normals to the surfaces $i+1/2$, j, k, $i, j+1/2$, k and i, j, $k+1/2$ whose absolute values are equal to their areas.

The difference fluxes $(\mathbf{H}\cdot\mathbf{S})^{n+1}_{i+1/2}$, $(\mathbf{H}\cdot\mathbf{S})^{n+1}_{j+1/2}$, and $(\mathbf{H}\cdot\mathbf{S})^{n+1}_{k+1/2}$ in (5), in accordance with the splitting of $\mathbf{H}$ in (4), are presented as the sums of inviscid and viscid difference fluxes

$$(\mathbf{H}\cdot\mathbf{S})_{m+1/2} = (\mathbf{H}^{\mathrm{in}}\cdot\mathbf{S})_{m+1/2} + (\mathbf{H}^{\mathrm{vis}}\cdot\mathbf{S})_{m+1/2} \qquad (m = i, j, k).$$

Since the introduction of artificial compressibility into the continuity equation transforms the type of the inviscid part of the Navier–Stokes equations to hyperbolic, the inviscid difference fluxes are calculated in accordance with the theory of high-order quasi-monotonic difference schemes for nonlinear hyperbolic systems of equations (TVD schemes) [11, 12]:

$$(\mathbf{H}^{\mathrm{in}}\cdot\mathbf{S})_{m+1/2} = \frac{1}{2}[(\mathbf{H}^{\mathrm{in}}_m + \mathbf{H}^{\mathrm{in}}_{m+1})\cdot\mathbf{S}_{m+1/2} - |\mathbf{A}|_{m+1/2}\Delta_{m+1/2}\mathbf{Q}] - \mathbf{W}_{m+1/2}. \tag{6}$$

Here $|\mathbf{A}| = \mathbf{A}^+ - \mathbf{A}^-$ and $\Delta_{m+1/2}\mathbf{Q} = \mathbf{Q}_{m+1} - \mathbf{Q}_m$. The term $\mathbf{W}_{m+1/2}$ in (6) is added to the first-order difference flux (enclosed in square brackets) to increase the approximation of the scheme to the third order. The term $\mathbf{W}_{m+1/2}$ contains TVD limiters, which ensure the minimum necessary level of dissipation and allow one to avoid artificial dissipative terms in the initial equations.

The matrices $\mathbf{A}^+$ and $\mathbf{A}^-$ entering into (6) are the components of the Jacobian of the inviscid flow

$$\mathbf{A} = \frac{\partial(\mathbf{H}^{\mathrm{in}}\cdot\mathbf{S})}{\partial\mathbf{Q}} = \mathbf{A}^+ + \mathbf{A}^-, \tag{7}$$

which have nonnegative and nonpositive eigenvalues, respectively.

The Jacobian $\mathbf{A}$ can be split into a sum of constant-sign matrices by different methods. The optimal splitting from the viewpoint of the number of arithmetic operations in the numerical algorithm proposed and the stability margin is

$$\mathbf{A}^{\pm} = 0.5(\mathbf{A} \pm \rho\mathbf{I}),$$

where $\mathbf{I} = \mathrm{diag}(1, 1, 1, 1)$, $\rho = |U| + \sqrt{U^2 + \mathbf{S}\cdot\mathbf{S}}$ is the spectral radius of the matrix $\mathbf{A}$, and $U = \mathbf{u}\cdot\mathbf{S}$.

The components of the viscous stress tensor in $(\mathbf{H}^{\mathrm{vis}}\cdot\mathbf{S})_{m+1/2}$ are calculated using the velocity components averaged over the values from the neighboring cells and the second-order central-difference formulas.

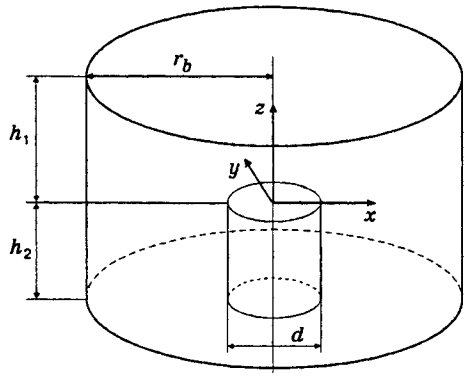

Fig. 1

Using linearization of (5) and (6) and approximate factorization of the resultant implicit operator arising in doing so, we obtain a system of linear equations

$$(\mathbf{B} - \mathbf{C}^+_{i-1/2}T_i^- - \mathbf{C}^+_{j-1/2}T_j^- - \mathbf{C}^+_{k-1/2}T_k^-) \cdot \mathbf{B}^{-1} \cdot (\mathbf{B} + \mathbf{C}^-_{i+1/2}T_i^+ + \mathbf{C}^-_{j+1/2}T_j^+ + \mathbf{C}^-_{k+1/2}T_k^+)\Delta\psi^{n+1} = \mathbf{RHS}^n_{ijk},$$

where

$$\mathbf{C}^\pm_{m+1/2} = \mathbf{A}^\pm_{m+1/2} \pm \frac{1}{\mathrm{Re}}\alpha_{m+1/2}\mathbf{D}, \qquad \alpha_{m+1/2} = \frac{\mathbf{S}_{m+1/2} \cdot \mathbf{S}_{m+1/2}}{V_{m+1/2}},$$

$$\mathbf{D} = \mathrm{diag}\,[0,1,1,1], \qquad V_{m+1/2} = 0.5(V_m + V_{m+1}), \qquad \Delta\psi^{n+1} = \mathbf{Q}^{n+1} - \mathbf{Q}^n,$$

$$\mathbf{B} = \mathbf{R}\frac{V_{ijk}}{\Delta t} + \frac{1}{\mathrm{Re}}\sum_{m=i,j,k}(\alpha_{m-1/2} + \alpha_{m+1/2})\mathbf{D} + 0.5\sum_{m=i,j,k}(\rho_{m-1/2} + \rho_{m+1/2})\mathbf{I},$$

$T_m^\pm$ are the operators of unit shift along the grid nodes forward (plus) or backward (minus) over the subscript m ($m = i$, j, and k) from the node i, j, k.

The system is solved by two fractional steps. At the first step, a single passage over the computational domain is performed in the ascending order of all subscripts:

$$\Delta\psi^*_{ijk} = \mathbf{B}^{-1}(\mathbf{RHS}^n_{ijk} + \mathbf{C}^+_{i-1/2}\Delta\psi^*_{i-1jk} + \mathbf{C}^+_{j-1/2}\Delta\psi^*_{ij-1k} + \mathbf{C}^+_{k-1/2}\Delta\psi^*_{ijk-1}).$$

The reverse direction is chosen at the second step:

$$\Delta\psi^{n+1}_{ijk} = \Delta\psi^*_{ijk} - \mathbf{B}^{-1}(\mathbf{C}^-_{i+1/2}\Delta\psi^{n+1}_{i+1jk} + \mathbf{C}^-_{j+1/2}\Delta\psi^{n+1}_{ij+1k} + \mathbf{C}^-_{k+1/2}\Delta\psi^{n+1}_{ijk+1}).$$

Since the matrix $\mathbf{B}$ is diagonal, its inversion is performed using an economic scalar procedure.

1.2. *Computational Domain.* The air flow is numerically simulated in the present work only in the vicinity of a cylindrical thin-walled input tube and inside it, the effect of the whole probe on the flow being ignored. Therefore, the cylindrical domain shown in Fig. 1 was used as a computational domain. It has the following parameters: d is the tube diameter, r_b is the radius of the cylindrical boundary, which is the external lateral boundary, and h_1 and h_2 are the distances from the input edge of the tube to the upper and lower external boundaries of the computational domain, respectively. The values of r_b, h_1, and h_2 are chosen rather large so that the disturbances from the tube do not reach the external (far) boundaries.

1.3. *Boundary Conditions.* The so-called nonreflecting boundary conditions are set at the far boundaries $z = h_1$, $z = h_2$, and $r = r_b$. These boundary conditions are based on hyperbolicity of the inviscid part of modified equations (4) (the effect of viscosity on the flow far from the solid walls is assumed to be insignificant). This approach allows us to avoid accumulation of spurious perturbations in the course of iterations inside the computational domain.

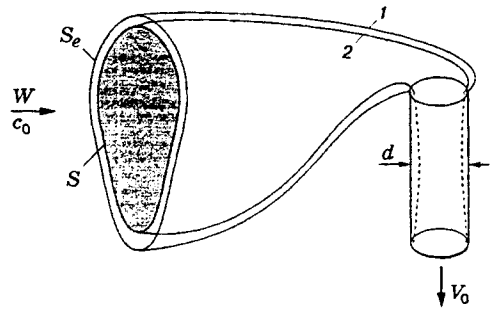

Fig. 2

The no-slip conditions are set on the solid walls for velocity and the projection of the pressure gradient onto the normal to the wall is assumed equal to zero.

The pressure that ensures a required flow rate of the air through the probe is specified at the lower butt-end of the tube through which the air enters the metering device of the probe. The velocity components are found by extrapolation of their values from the internal part of the computational domain.

1.4. *Calculation of Trajectories of Individual Particles and Aspiration Efficiency.* The particle trajectories are calculated by solving the equation of motion written under the assumption that the resistance of air to a particle satisfies the Stokes law

$$m\frac{d\mathbf{u}}{dt} = \frac{3\pi\mu d_p}{C_C}(\mathbf{v}-\mathbf{u}),$$

where m and d_p are the particle mass and diameter, $\mathbf{v}$ is the velocity of the air, $\mathbf{u}$ is the particle velocity, μ is the viscosity of the air, and C_C is the Cunningham correction for molecular slipping. Using the tube-orifice diameter d and the free-stream velocity W as the characteristic length and velocity, we can rewrite the above equation in the dimensionless form

$$\mathrm{Stk}\frac{d\mathbf{u}'}{dt'} = \mathbf{v}'-\mathbf{u}', \tag{8}$$

where $\mathrm{Stk} = \rho_p C_C d_p^2 W/(18\mu d) = \tau W/d$ is the Stokes number, $\mathbf{v}' = \mathbf{v}/W$ and $\mathbf{u}' = \mathbf{u}/W$ are the dimensionless velocities of the air and the particle, $t' = tW/d$ is the dimensionless time, and τ is the particle relaxation time.

Equation (8) is integrated by the fourth-order Runge–Kutta method. The trajectory begins from a certain chosen starting point sufficiently far from the tube so that the air could be considered as undisturbed and ends if the particle entered the tube, touched the wall (the particle size is ignored), or flew past the tube.

The efficiencies of external and total aspiration are calculated as the ratios of the concentrations c_e and c of the particles that enter only the input orifice of the tube and reach the output cross section, respectively, to the particle concentration c_0 in an undisturbed flow far upstream from the tube.

Two tubes of particle trajectories are depicted in Fig. 2, which shows schematically the aspiration process. The surface of the external tube 1 is the set of limiting trajectories of particles that still enter the input tube. The particles located outside of this surface do not enter the tube. The surface of the internal tube 2 is formed by the limiting trajectories of the particles reaching the output cross section of the tube.

Let S_e and S be the cross-sectional areas of the internal and external tubes of particle trajectories in the plane located in an undisturbed flow far upstream from the input tube of the probe perpendicular to the free-stream velocity vector. The particle concentration in the free stream is c_0. Equating the particle fluxes through the cross sections S_e and S to the fluxes through the input and output cross sections of the tube, we obtain

$$c_0 W S_e = c_e Q, \qquad c_0 W S = cQ, \tag{9}$$

where $Q = 0.25\pi d^2 V_0$ is the volume flow rate of the air in the tube. According to the definitions of the total and external aspiration (1) and (2), we obtain from (9)

$$A = \frac{c}{c_0} = \frac{4WS}{\pi d^2 V_0}, \qquad A_e = \frac{c_e}{c_0} = \frac{4WS_e}{\pi d^2 V_0}.$$

Thus, the calculation of the efficiencies of the total and external aspiration after determination of the velocity field of the air and the set of particle trajectories reduces to determination of the areas S and S_e of the cross sections of the tubes of particle trajectories that enter the output and input cross sections of the probe.

If the free-stream direction is parallel to the probe axis (see, for example, [13, 14], where the coaxial aspiration is studied numerically by solving two-dimensional Navier—Stokes equations), the problem is symmetrical, and it is sufficient to find one limiting trajectory bounding the particles that enter the tube using the method of halving.

In our case, the shape of the desired cross section is rather complicated, as shown below, and the value of S was found by simple exhaustion of the starting points of the calculated trajectories and by summation of the vicinities of the starting points of those particles that enter the tube.

2. Assumptions Adopted in Calculation of the Aspiration Efficiency. The aspiration efficiency in a thin-walled tube depends on the following parameters: free-stream velocity W, mean suction velocity of the air in the tube V_0, tube diameter d, particle diameter d_p, particle density ρ_p, air density ρ_a, air viscosity μ, and the angle between the free-stream direction and the tube axis α. According to the theory of dimension [15], a function of eight variables that include three dimensions (mass, length, and time) can be transformed to a function of $8 - 3 = 5$ dimensional groups

$$A = f(\mathrm{Stk}, R, \mathrm{Re}, \mathrm{Re}_p, \alpha),$$

where $R = W/V_0$, $\mathrm{Re} = \rho_a W d/\mu$ is the Reynolds number, and $\mathrm{Re}_p = \rho_a W d_p/\mu$ is the Reynolds number of the particle.

If $\mathrm{Re}_p \ll 1$, the resistance of the air to the particle satisfies the Stokes law with good accuracy. In accordance with Eq. (8), the particle motion is determined by the Stokes number and does not depend on the Reynolds number. The particle can be assigned an equivalent aerodynamic diameter, which is defined as the diameter of a spherical particle of unit density that has the same steady velocity of gravitational deposition in steady air. It is shown in a number of experimental [7] and theoretical [13, 14] publications that the Reynolds numbers of the tube Re and the particle Re_p weakly affect the aspiration efficiency (the maximum error was 7%). Therefore, the aspiration efficiency was determined in the present work as a dependence of the form

$$A = f(\mathrm{Stk}, R, \alpha),$$

and the Reynolds number of the tube Re was fixed.

The dependence of the aspiration efficiency on Re and Re_p, and the ranges of velocities of the air and the tube and particle sizes, for which the Reynolds number effect can be ignored, require further investigation.

3. Calculation Results. The aspiration efficiency into a tube of diameter $d = 0.01$ m was calculated for the free-stream velocity $W = 5$ m/sec. The Reynolds number corresponding to these parameters was $\mathrm{Re} = 3450$. The mean velocity of air suction in the tube V_0 varied within 1.7 to 20 m/sec, and the Stokes number varied from 0.01 to 0.40.

In the course of preliminary calculations, we chose the values $r_b = 18d$ and $h_1 = h_2 = 10d$, whose subsequent increase did not affect the solution obtained. The calculations on a sequence of grids allowed us to choose the optimal number of nodes of the general grid: 54 nodes in the radial direction, 47 nodes over the height of the computational domain (Oz axis), and 20 nodes in the circumferential direction. The results presented below were obtained for these parameters of the domain and the grid.

Figure 3 shows the air-flow pattern (streamlines) in the vicinity of the input tube of the probe and inside it for $V_0 = 10$ m/sec (which corresponds to the volume flow rate of the air through the tube $Q = 0.785$ liter/sec).

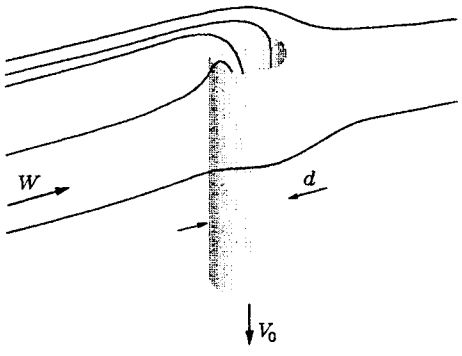

Fig. 3

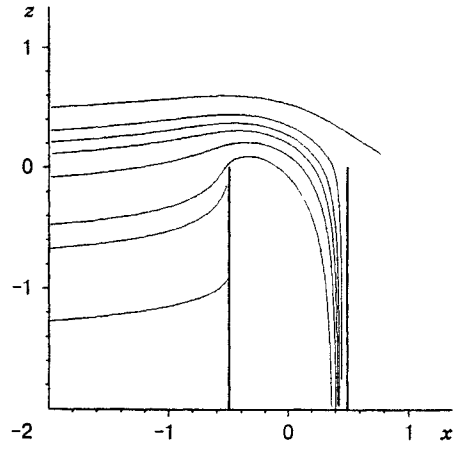

Fig. 4

Fig. 5

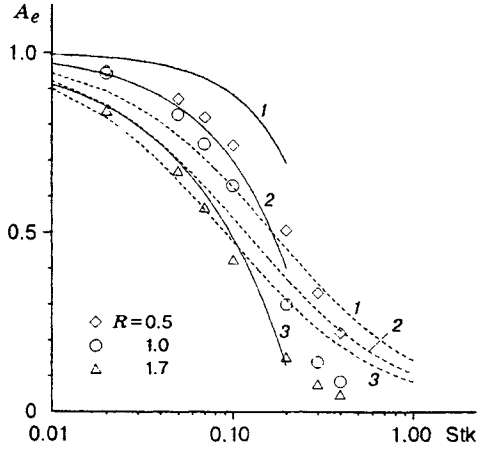

Fig. 6

Figure 4 shows some particle trajectories for $V_0 = 10$ m/sec and Stokes number Stk $= 0.1$ in the plane of symmetry of the problem $y = 0$. A zone adjacent to the upwind surface of the tube, wherein the particles do not hit due to their inertia, is observed inside the tube. Therefore, the deposition of the particles onto the metering device occurs very nonuniformly, with the maximum concentration of the particles at the downwind side of the tube.

The calculated values of the external A_e and total A aspiration efficiency for different values of V_0 and Stk are listed in Table 1.

Figure 5 shows cross sections of the limiting tubes of particle trajectories, which enter the input cross section of the tube. They were obtained for different values of V_0 and Stk. To compare the size, we projected the contour of the input tube of the probe onto these cross sections. Under each cross section, the corresponding value of the external aspiration A_e is given. Narrow bands of "clearance" on the background of these cross sections at rather high values of V_0, which correspond to particle trajectories that do not enter the probe, should be noted. At the same time, a certain number of particles outside these bands are sucked into the tube. The mechanism of this phenomenon is as follows. At rather high values of V_0, particle trajectories turning upstream due to the suction of particles into the probe appear above the input cross section of the tube. The

TABLE 1

Stk	V_0, m/sec							
	1.7	3.0	5.0	7.0	10.0	14.0	17.0	20.0
				A_e				
0.010	0.865	0.888	0.984	0.918	0.976	0.951	0.918	0.938
0.020	0.790	0.835	0.943	0.889	0.951	0.932	0.901	0.923
0.050	0.575	0.668	0.828	0.798	0.874	0.868	0.844	0.867
0.070	0.452	0.566	0.747	0.738	0.822	0.824	0.803	0.825
0.100	0.307	0.421	0.631	0.652	0.744	0.757	0.741	0.763
0.200	0.100	0.148	0.299	0.387	0.507	0.553	0.554	0.585
0.300	0.036	0.073	0.139	0.205	0.332	0.398	0.436	0.450
0.400	0.004	0.044	0.084	0.116	0.221	0.293	0.313	0.378
				A				
0.010	0.849	0.876	0.981	0.918	0.976	0.951	0.918	0.938
0.020	0.771	0.819	0.936	0.888	0.951	0.932	0.901	0.923
0.050	0.535	0.631	0.806	0.791	0.874	0.868	0.844	0.867
0.070	0.387	0.495	0.702	0.723	0.822	0.824	0.783	0.825
0.100	0.206	0.274	0.497	0.602	0.742	0.757	0.726	0.763
0.200	0.016	0.020	0.021	0.017	0.019	0.135	0.176	0.269
0.300	0	0.003	0.003	0.001	0.003	0.006	0.039	0.082
0.400	0	0	0.001	0.001	0.001	0.002	0.009	0.049

particles flying closer to the input cross section do not have enough time to turn in order to enter the probe and hit the downwind side of the tube near the leading edge. The totality of these particles constitute the "clearance" in the cross section of the limiting tube of particle trajectories. The particles flying above the latter experience turning along a more distant trajectory and have enough time to turn and enter the probe tube.

On the basis of experimental data, Hangal and Willeke [5] derived a semi-empirical relationship for the aspiration efficiency into a cylindrical tube located at an angle α to the incoming flow

$$A = 1 + 3(R\cos\alpha - 1)\mathrm{Stk}^{\sqrt{R}}, \tag{10}$$

which approximates the experimental values of the aspiration efficiency on the following intervals of the parameters entering into it: $0.02 \leqslant \mathrm{Stk} \leqslant 0.20$, $0.5 \leqslant R \leqslant 2.0$, and $45° \leqslant \alpha \leqslant 90°$.

In turn, Vincent [2] proposed the formula

$$A = 1 + \left[1 - \frac{1}{1 + G(\alpha)\mathrm{Stk}\,(\cos\alpha + 4\sqrt{R\sin\alpha})}\right](R\cos\alpha - 1),$$

which is simplified for $\alpha = 90°$ and has the following form for the value of the coefficient G obtained by Vincent as a result of analysis of experimental data:

$$A = \frac{1}{1 + 8.4\,\mathrm{Stk}\,R^{0.5}}. \tag{11}$$

Figure 6 shows the aspiration efficiency as a function of Stk for different values of the parameter R, which were obtained from formulas (10) (solid curves) and (11) (dashed curves); the points refer to the external aspiration efficiency calculated by the method proposed in the present work. Curves 1–3 correspond to $R = 0.5$, 1.0, and 1.7. The calculation data are in reasonable agreement with formula (10) for $R = 1.7$ and 1, i.e., for low suction velocities $V_0 = 3$ and 5 m/sec. Greater differences are observed for $R = 0.5$ and $V_0 = 10$ m/sec. This is possibly related to the fact that the experimental data approximated by formula (10)

were affected by secondary aspiration, i.e., the suction of particles that recoil from the external surface of the tube. This effect is usually manifested at high values of the velocity of the air at the tube input and small R when the air is sucked into the tube from a wide spatial region. In the calculations, the particles that touched the tube surface were considered to be lost. The data obtained are also in qualitative agreement with formula (11). On one hand, this formula is derived on the basis of a theoretical model that ignores the secondary aspiration; on the other hand, it includes the coefficient G obtained from a large range of experimental data possibly affected by secondary aspiration. Thus, with account of the large scatter of experimental data and difficulties in their interpretation, the results obtained seem quite satisfactory. Experimental verification of the proposed mathematical model will possibly require a higher level of experiments.

Conclusion. A universal method for calculation of the aspiration efficiency for real configurations of the probes has been proposed. The calculations performed have demonstrated the effectiveness and reliability of the method. It is planned to extend this method to study the processes of aspiration into tubes oriented at different angles to the flow, probes of different shapes, and also aspiration from turbulent flows.

This work was partly supported by the Russian Foundation for Fundamental Research (Grant Nos. 96-01-01934 and 98-01-00742).

REFERENCES

1. G. N. Lipatov, G. L. Shingarev, S. A. Grinshpun, and A. G. Sutugin, "Aspiration of aerosol from an air flow into a slotted probe," *Izv. Akad. Nauk SSSR, Fiz. Atmos. Okeana*, **23**, No. 3, 320–323 (1987).
2. J. H. Vincent, *Aerosol Sampling: Science and Practice*, Wiley, New York (1989).
3. A. G. Laktionov, "Aspiration of aerosol in a vertical tube from a transverse flow," in: *Tr. Mosk. Inst. Prikl. Geofiz.*, No. 7, 83–87 (1973).
4. M. D. Durham and D. A. Lundgren, "Evaluation of aerosol aspiration efficiency as a function of Stokes number, velocity ratio, and nozzle angle," *J. Aerosol Sci.*, **11**, No. 2, 179–188 (1980).
5. S. Hangal and K. Willeke, "Overall efficiency of tubular inlets sampling at 0–90 degrees from horizontal aerosol flows," *Atmos. Environ.*, **24**, No. 9, 2379–2386 (1990).
6. S. P. Belyaev and L. M. Levin, "Experimental study of aerosol aspiration," in: *Tr. Obninsk Inst. Éxp. Meteorology*, No. 20, 3–33 (1971).
7. G. N. Lipatov, S. A. Grinshpun, G. L. Shingaryov, and A. G. Sutugin, "Aspiration of coarse aerosol by a thin-walled sampler," *J. Aerosol Sci.*, **17**, No. 5, 763–769 (1986).
8. Yu. A. Gryazin, S. G. Chernyi, S. V. Sharov, and P. A. Shashkin, "Method of numerical solution of three-dimensional problems of incompressible fluid dynamics," *Dokl. Ross. Akad. Nauk*, **353**, No. 4, 478–483 (1997).
9. N. A. Vladimirova, B. G. Kuznetsov, and N. N. Yanenko, "Numerical simulation of viscous incompressible flow past a flat plate," in: *Some Problems of Computational and Applied Mathematics* [in Russian], Nauka, Novosibirsk (1966), pp. 186–192.
10. A. J. Chorin, "A numerical method for solving incompressible viscous flow problems," *J. Comput. Phys.*, **2**, 12–26 (1967).
11. A. Harten, "High resolution schemes for hyperbolic conservation laws," *J. Comput. Phys.*, **49**, 357–393 (1983).
12. S. R. Chakravarthy and S. Osher, "A new class of high accuracy TVD schemes for hyperbolic conservation laws," AIAA Paper No. 363, 1–11 (1985).
13. D. J. Rader and V. A. Marple, "A study of the effects of anisokinetic sampling," *Aerosol Sci. Technol.*, No. 8, 283–299 (1988).
14. B. Y. H. Liu, Z. O. Zhang, and T. H. Kuehn, "A numerical study of inertial errors in anisokinetic sampling," *J. Aerosol Sci.*, **20**, No. 3, 367–380 (1989).
15. E. Buckingham, "On physically similar systems: illustrations of the use of dimensional equations," *Phys. Rev.*, **2**, No. 4, 345 (1914).